Frontiers in Bioscience Landmark

Front. Biosci. (Landmark Ed) **2026**; 31(8): 53391
https://doi.org/10.31083/FBL53391

Original Research

Targeting the HIF-1α/IL-1β Axis in Macrophages With the Novel Inhibitor LJ-6 Mitigates Adipose Tissue Inflammation in Cellular and *Ex Vivo* Models

Min Gao[1,2,3], Mengyuan Liu[4], Anran Chu[4], Sisi Deng[5,6], Jingsong Gao[4], Shasha Li[4], Dongsheng Jiang[4], Yuqing Shen[4], Xinyue Wang[4], Saifei Lei[1,3], Rui Wu[1,3], Haowen Jiang[2,3], Jia Li[1,2,3], Jinlong Li[4], Xinyi Wang[2,3,*], Chang Peng[1,*]

[1]Key Laboratory of Glyco-drug Research of Zhejiang Province, School of Pharmaceutical Science and Technology, Hangzhou Institute for Advanced Study, University of Chinese Academy of Sciences, 310024 Hangzhou, Zhejiang, China
[2]State Key Laboratory of Chemical Biology, Shanghai Institute of Materia Medica, Chinese Academy of Sciences, 201203 Shanghai, China
[3]University of Chinese Academy of Sciences, 100049 Beijing, China
[4]School of Pharmacy, Nantong University, 226001 Nantong, Jiangsu, China
[5]College of Integrated Traditional Chinese and Western Medicine, Hunan University of Chinese Medicine, 410128 Changsha, Hunan, China
[6]Key Laboratory of Hunan Province for Integrated Traditional Chinese and Western Medicine on Prevention and Treatment of Cardio-Cerebral Diseases, College of Integrated Traditional Chinese and Western Medicine, Hunan University of Chinese Medicine, 410128 Changsha, Hunan, China
*Correspondence: wxy_sydney@163.com (Xinyi Wang); pengchang@ucas.ac.cn (Chang Peng)
Academic Editor: Pietro Gentile
Submitted: 29 April 2026 Revised: 30 June 2026 Accepted: 21 July 2026 Published: 21 August 2026

Abstract

Background: Sustained activation of adipose tissue macrophages (ATMs) drives metabolic dysfunction in obesity, with the hypoxia-inducible factor-1α (HIF-1α)/interleukin-1β (IL-1β) axis being a core signaling pathway. However, specific strategies targeting this axis are still lacking. Here, we aimed to identify novel compounds capable of disrupting this pathway. **Methods:** We screened a natural product library for inhibitors of IL-1β expression in macrophages. The hit compound LJ-6 was then evaluated in lipopolysaccharide (LPS)-stimulated bone marrow-derived macrophages (BMDMs) and in a physiologically relevant model using conditioned medium from obese adipose tissue. Mechanism of action was investigated *via* Western blotting, molecular docking, dynamics simulations, and hypoxia-response element (HRE)-luciferase reporter assays with site-directed mutagenesis. **Results:** LJ-6 was identified as a potent inhibitor of IL-1β. It dose-dependently suppressed IL-1β in both LPS-induced and obese adipose tissue-conditioned medium-induced macrophage inflammation. Mechanistically, LJ-6 reduced HIF-1α protein stability. Molecular docking and mutagenesis studies supported an interaction involving the Tyr92 and His197 residues of HIF-1α, and suggested that this interaction is critical for its inhibitory function on the HIF-1α/IL-1β axis. **Conclusions:** This study identifies the natural compound LJ-6 as a novel direct inhibitor of HIF-1α. By binding to HIF-1α, LJ-6 effectively suppresses the HIF-1α/IL-1β axis in macrophages, thereby reducing IL-1β-driven inflammatory responses in cellular and *ex vivo* models of obesity-associated adipose tissue inflammation, and thus represents a promising lead compound for therapeutic development.

Keywords: adipose tissue; inflammation; hypoxia-inducible factor 1, alpha subunit; LJ-6; interleukin-1beta; macrophages

1. Introduction

Obesity, characterized by pathological lipid accumulation in adipose tissue, has become a major global public health challenge [1]. Beyond its effects on body shape, it elevates the development of metabolic diseases, including cardiovascular disorders, type 2 diabetes, non-alcoholic fatty liver disease, and hypertension, imposing a substantial health and socioeconomic burden [2,3,4]. Obesity is now recognized not merely as a disorder of energy balance, but as a chronic, low-grade systemic inflammatory disease [5]. This inflammation originates in pathologically remodeled adipose tissue. In obesity, adipocyte hypertrophy gives rise to local relative hypoxia and cellular stress [6]. Immune cells, particularly macrophages, infiltrate the tissue. These adipose-tissue macrophages (ATMs) undergo activation, adopt a pro-inflammatory phenotype, and secrete inflammatory cytokines such as tumor necrosis factor-α (TNF-α) and IL-1β [7,8]. This inflammatory environment impairs insulin signaling in adipocytes and promotes systemic insulin resistance, thereby disrupting metabolic homeostasis [9]. Targeting ATM-driven inflammation is therefore a promising therapeutic strategy.

Although current anti-obesity drugs, including glucagon-like peptide-1 (GLP-1) receptor agonists, effectively reduce weight, they may not completely reverse established adipose tissue inflammation [10]. Even after weight loss, abnormal ATMs activation and inflammatory memory may persist, potentially contributing to weight regain [11,12]. Thus, therapeutic strategies that directly

target adipose inflammation are needed to complement current weight-management approaches.

Among inflammatory mediators from ATMs, IL-1β plays a central role [13,14]. Genetic studies have shown that macrophage-specific deletion of IL-1β, but not TNF-α, prevents the development of diet-induced obesity and insulin resistance in mice [15,16]. Clinically, inhibitors of the IL-1β pathway improve glycemic control and lower cardiovascular risk [13,17], underscoring IL-1β as a key node linking obesity, inflammation, and metabolic dysfunction.

Direct neutralization of IL-1β carries a potential risk of increasing susceptibility to infections [18]. Targeting upstream regulators of its production may therefore provide a safer therapeutic strategy. In this context, hypoxia-inducible factor-1α (HIF-1α) represents a compelling target, as it is stabilized in the hypoxic adipose tissue of obesity and acts as a key transcriptional driver of IL-1β in macrophages [19]. Pharmacological or genetic inhibition of HIF-1α has been shown to attenuate adipose tissue inflammation and improve metabolic parameters, supporting its involvement in the obesity–hypoxia–inflammation cycle [20]. Our previous work further established that activation of the HIF-1α/IL-1β axis in ATMs exacerbates local inflammation and accelerates metabolic dysfunction, reinforcing this axis as a promising target for intervention [16]. However, existing small-molecule inhibitors of HIF-1α lack the selectivity or safety profile required for chronic metabolic diseases, highlighting the need for novel and specific modulators of this pathway.

To address this gap, we turned to the rich chemical space of natural products, which have long been recognized as a prolific source of bioactive compounds with favorable biocompatibility [21]. We hypothesized that this resource could yield novel agents capable of selectively inhibiting the HIF-1α/IL-1β axis in macrophages, thereby alleviating obesity-associated inflammation. Here, we report the discovery and mechanistic characterization of LJ-6, a natural compound identified in this IL-1β-directed screen, which directly targets HIF-1α to suppress IL-1β expression.

2. Materials and Methods

2.1 Preliminary Screening of Natural Products for Anti-Inflammatory Activity

A library of 42 natural products, encompassing diverse structural classes such as alkaloids, triterpenoids, flavonoids, and lignans, was preliminarily screened for their ability to suppress inflammatory activation in macrophages. RAW 264.7 cells (#TIB-71, ATCC), a murine macrophage line with the passages 5–10, were employed as the screening platform. The RAW 264.7 were authenticated by STR profiling, and tested negative for mycoplasma. The culture medium consisted of Dulbecco's Modified Eagle Medium (DMEM) (#12800082, Gibco) supplemented with 10% fetal bovine serum (FBS) (#10091-148, Gibco) and penicillin (100 U/mL)-streptomycin (100 μg/mL) (#15140-122, Gibco) and cells were cultured at 37 °C with 5% CO_2. At ~90% confluence, cells were placed in 24-well plates at a density of 1.5×10^5 cells/well and cultured for attachment for 12 h. For compound treatment, RAW 264.7 were pretreated for 12 h using each test compound (5 μM) and the reference inhibitor BAY 11-7082 (5 μM; #HY-13453, MedChemExpress). Then, inflammatory activation was stimulated using 100 ng/mL lipopolysaccharide (LPS, #L2630, Sigma) for a further 12 h. After stimulation, the expression of key inflammatory genes was measured to evaluate the inhibitory activity of the natural product library (**Supplementary Table 1**, Supporting Information).

The percentage inhibition of IL-1β mRNA expression was calculated relative to the LPS-only control group. Compounds that achieved ≥50% inhibition were classified as "hits", while those showing 25% to <50% inhibition were designated as having "modest activity". Compounds with <25% inhibition were considered inactive.

2.2 Derivation of BMDMs From Bone Marrow

Bone marrow cells were flushed from the femurs and tibiae of 8-week-old mice using phosphate-buffered saline (PBS), prepared in-house with NaCl (9 g/L) [#10019318, Sinopharm], KH_2PO_4 (0.144 g/L) [#10017608, Sinopharm], and Na_2HPO_4 (0.42 g/L) [#20040617, Sinopharm] at pH 7.4. The harvested cell suspension was centrifuged at 500 ×g for 5 minutes, and the resulting pellet was treated with 1 mL of red blood cell lysis buffer [#B541001, Sangon Biotech (Shanghai) Co., Ltd] for 5 min to remove erythrocytes, followed by a second centrifugation step (500 ×g, 5 minutes). The remaining bone marrow cells were then resuspended in culture medium composed of DMEM supplemented with 10% FBS, penicillin (100 U/mL) and streptomycin (100 μg/mL), and 20 ng/mL macrophage colony-stimulating factor (M-CSF) [#RP01216, ABclonal], seeded into culture plates, and maintained at 37 °C in a 5% CO_2 humidified incubator. Fresh medium was supplied every 48 h, and differentiated bone marrow-derived macrophages (BMDMs) were harvested on day 7 of culture.

The mature bone marrow-derived macrophages were validated for their identity by surface marker (F4/80) analysis using flow cytometry (see **Supplementary Fig. 1** of Supplementary Materials for detailed results) and tested negative for mycoplasma. The flow cytometry analysis was performed in the following steps: Mature BMDMs were subjected to a single wash with Dulbecco's phosphate-buffered saline (DPBS) (#554656, BD Pharmingen), then cells were resuspended in 100 μL DPBS supplemented with 2 μL Fc receptor blocking reagent (#553142, BD Pharmingen) and kept at 4 °C for 15 min. Subsequently, 100 μL of DPBS containing 2 μL of the F4/80 antibody (#565410, BD Pharmingen) was added to the blocking mixture, and the incubation was prolonged for a further 30 min at the

same temperature. Finally, the cells were washed twice with DPBS, re-suspended in 500 µL DPBS, and analyzed on a CytoFLEX S flow cytometer (Beckman Coulter).

2.3 Macrophage Activation

To induce pro-inflammatory activation in macrophage, cells were exposed to 100 ng/mL LPS for designated time intervals, after which intracellular mRNA and protein levels were assessed. For IL-1β secretion analysis, cells were first primed with LPS (100 ng/mL) for 12 h, followed by a 30-minute incubation with ATP (2 mM) [#HYB2176, MCE] to trigger inflammasome-mediated release. The amount of IL-1β present in the culture supernatant was then quantified using a mouse IL-1β-specific enzyme-linked immunosorbent assay kit [#RK00006, ABclonal].

2.4 Obtaining Conditioned Medium From Adipose Tissue

Epididymal fat pads (2 g) harvested from either chow-fed lean or high-fat diet (HFD)-fed obese C57BL/6J mice were minced and subjected to enzymatic dissociation in 10 mL of DMEM containing Collagenase D (2 mg/mL) [#11088882001, Roche], Dispase II (2.4 mg/mL) [#4942078001, Roche], and $CaCl_2$ (10 mM) [#10005817, Sinopharm] at 37 °C for 1 hour. Digestion was terminated by the addition of 10 mL of DMEM supplemented with 20% FBS, and the cell suspension was passed through a 40-µm mesh filter. Following centrifugation at 500 ×g for 10 min, the floating adipocyte layer and the pelleted stromal vascular fraction were discarded, while the intervening supernatant was retained as adipose tissue-conditioned medium (AT CM). For macrophage stimulation, this AT CM was diluted with fresh culture medium at a 1:3 ratio (AT CM:medium) before application to BMDMs for the indicated durations.

The collected conditioned media were used directly without further dilution or concentration. Notably, the healthy and obese AT CM were prepared under strictly identical conditions, including tissue weight, digestion volume, and processing time, and were applied to BMDMs in parallel. Therefore, any differential effects observed between the two CM groups can be attributed to the distinct inflammatory milieu of the adipose tissues rather than procedural variability.

2.5 RNA Extraction and Real-Time Quantitative PCR Analysis

Total RNA was extracted from cultured cells using TRIzol-based methodology. Briefly, cells were lysed in 300 µL of TRIzol reagent [#15596018, Invitrogen] on ice for 15 minutes, followed by the addition of 60 µL of chloroform [#10006818; Sinopharm] and vigorous vortexing for 15 seconds. Phase separation was achieved by centrifugation at 12,000 ×g for 15 minutes, and the aqueous upper phase was transferred to a fresh tube. RNA was precipitated by mixing the recovered aqueous phase with 150 µL of isopropanol [#80109218; Sinopharm], vortexed briefly, and kept at –20 °C overnight. The precipitated RNA was collected by centrifugation (12,000 ×g, 15 minutes), washed twice with 70% ethanol [#10009218; Sinopharm], and centrifuged again at 7500 ×g for 10 minutes. After air-drying, the RNA pellet was dissolved in 20 µL of RNase-free water, and its concentration was determined using a Nanodrop 2000 spectrophotometer (Thermo Fisher Scientific). For cDNA synthesis, 1 µg of total RNA was reverse-transcribed with the ABScript III RT Master Mix for qPCR [#RK20408, ABclonal] and diluted to a final volume of 180 µL with nuclease-free water. Quantitative PCR was performed in a 10-µL reaction mixture containing 4 µL of diluted cDNA, 1 µL of gene-specific primers (**Supplementary Table 3**), and 5 µL of 2 × Universal SYBRGreen Fast qPCR Mix [#RK21203, ABclonal]. Amplification was carried out on a QuantStudio system (Thermo Fisher Scientific) under the following cycling parameters: initial denaturation at 95 °C for 5 minutes, followed by 40 cycles of 95 °C for 30 seconds and 60 °C for 30 seconds. Raw threshold cycle (Ct) values were acquired using QuantStudio Software (v1.5.2), and relative transcript levels were calculated after normalization to the endogenous reference gene (β-actin).

2.6 Western blotting Assay

To prevent HIF-1α degradation, all lysis procedures were carried out on ice using SDS loading buffer freshly supplemented with a protease inhibitor cocktail [#HY-K0010, MedChemExpress]. Following two washes with PBS, cells were harvested in SDS loading buffer composed of 0.5 M Tris-HCl (pH 6.8, 20 mL) [#1610799, Bio-Rad], SDS (4 g) [#20106ES76, Yeasen], bromophenol blue (200 mg) [#71008060, Sinopharm], glycerin (20 mL) [#10010618, Sinopharm], and DTT (3.08 g) [#ST040, Beyotime] brought to a final volume of 200 mL with distilled water. The lysates were then heated at 100 °C for 10 minutes to achieve complete denaturation. Protein samples were resolved by SDS-PAGE using a running buffer (glycine 14.4 g/L [#60112ES96, Yeasen], Tris-base 3.02 g/L [#60102ES, Yeasen], SDS 1 g/L), and subsequently electrotransferred onto nitrocellulose membranes in transfer buffer (glycine 14.4 g/L, Tris-base 3.02 g/L, methanol 200 mL/L [#80080418, Sinopharm]). Following transfer, membranes were blocked for 1 hour at ambient temperature with 5% non-fat milk to minimize background signals. The blocked membranes were then probed with primary antibodies (**Supplementary Table 4**) overnight at 4 °C. After removal of the primary antibody solution, the membranes were rinsed three times (10 minutes each) with TBST [Tris-base 2.42 g/L, NaCl 8 g/L, HCl 1.6 mL/L [#10011028, Sinopharm], Tween-20 1 mL/L [#30189328, Sinopharm], pH 7.6] and subsequently incubated with secondary antibodies for 1 hour at room temperature. Immunoreactive bands were visualized using ECL detection

buffer [#MA0186, MeilunBio] and imaged with the Chemi-Doc system (Bio-Rad).

The density of protein was quantified using ImageJ software (v1.54p), and the relative protein expression level was calculated as the ratio of the target protein band intensity to the corresponding loading control (β-actin) band intensity, and the fold change was normalized to the control group.

2.7 Protein Structure Preparation and Molecular Dynamics Simulations

The initial protein structure was modeled using the Swiss-Model server (accession: Q16665_11-357:4zpk.1.B) [22]. To better approximate physiological conditions for subsequent molecular dynamics (MD) simulations and docking studies, the protein termini were capped with an N-acetyl (ACE) group at the N-terminus and an N-methylamide (NME) group at the C-terminus.

A cubic simulation box with periodic boundaries was constructed, and the protein was solvated using the TIP3P water model [23]. Neutralization of the system was performed, and NaCl was added to a final concentration of 150 mM to achieve physiological ionic strength. The Amber ff99SB*-ILDN force field [24,25,26,27] was applied to the protein, with ligand parameters derived from the General Amber Force Field (GAFF) [28]. System equilibration was performed with Desmond (v2023.4) [29] on a GPU, following a standard protocol involving NVT and NPT ensembles. Production MD simulations were conducted in the NPT ensemble at 310 K and 1.013 bar, maintained by the Nosé-Hoover thermostat [30] and the Martyna-Tobias-Klein barostat [31], respectively. A 2-fs time step was used with a multigrator scheme employing a modified r-RESPA integrator [32], where long-range electrostatics were evaluated every three steps. All simulations were carried out on an NVIDIA RTX-3080TI GPU for a total duration of 500 ns.

Analysis of the root-mean-square deviation (RMSD) trajectory indicated that the protein structure reached convergence after approximately 230 ns, remaining stable for the remainder of the simulation (230–500 ns, **Supplementary Fig. 4**, Supporting Information), with secondary structure elements preserved throughout. The final frame from the 500 ns trajectory was extracted and served as the receptor structure for subsequent molecular docking studies.

2.8 Molecular Docking and MM/GBSA-Based Binding Affinity Assessment

Global molecular docking was performed to explore potential binding modes of LJ-6. The receptor structure was prepared using AutoDockTools (v1.5.7). A docking grid of dimensions 81.9 × 81.9 × 81.9 $Å^3$ was centered on the protein to encompass the entire structural domain. Docking calculations were executed with AutoDock Vina [33,34], using an exhaustiveness value of 512 to generate 100 initial ligand conformational poses. Prior to docking, the initial geometry of LJ-6 was optimized using OpenBabel (v3.1.0) [35], and was subsequently processed with the Meeko toolkit [36] to ensure correct formatting for docking. Following the docking screening, 97 distinct ligand-receptor complex poses were obtained (**Supplementary Fig. 5**, Supporting Information).

The binding affinities of these complexes were further evaluated and refined using the MM/GBSA method as implemented in the gmx_MMPBSA.py tool [37,38]. This post-docking refinement protocol involved energy minimization followed by binding free energy scoring. To assess the stability of the predicted binding modes, each complex subsequently underwent a short 10-ns MD simulation (**Supplementary Table 2**, Supporting Information). The binding free energy was then re-calculated using the same MM/GBSA protocol on snapshots extracted from the equilibrated portion of these simulations.

Subsequently, the top 5 ranked conformations based on the MM/GBSA results were subjected to a prolonged 500 ns MD simulation using Desmond, employing the same simulation parameters as described above. The most stable conformation from this long-timescale simulation was selected for further in-depth analysis (**Supplementary Fig. 6**, Supporting Information).

2.9 Cellular Thermal Shift Assay

Mature BMDMs were pretreated with 100 ng/mL LPS for 12 hours to induce HIF-1α expression. Cells were then harvested and lysed in IP lysis buffer (#P0013, Beyotime) on ice for 30 minutes, followed by centrifugation at 12,000 ×g for 10 minutes at 4 °C to collect total protein lysates. The clarified lysates were divided into two aliquots and incubated with either DMSO (vehicle control) or 10 μM LJ-6 for 30 minutes at room temperature. Each sample was then further split into 50 μL aliquots and subjected to heating at the indicated temperatures for 3 minutes. After heating, the samples were centrifuged at 15,000 ×g for 30 minutes at 4 °C to remove precipitated aggregates, and the resulting soluble fractions were mixed with an equal volume of 2 × loading buffer and analyzed by Western blotting using an anti-HIF-1α antibody.

2.10 Luciferase Assay

293T cellswere seeded in a 10-cm dish and co-transfected with the HRE luciferase reporter plasmid and the HIF-1α expression plasmid using Lipofectamine 2000 (#11668019, Thermo Fisher Scientific). After 24 hours, the transfected cells were harvested and replated into a black-frame, clear-bottom 96-well plate. Following an additional 24-hour culture, the cells were treated with LJ-6 for 12 hours. Luciferase activity was then measured using the Steady-Lumi™ II Firefly Luciferase Reporter Gene Assay Kit (#RG059M, Beyotime) on a Multimode Plate Reader (EnVision, PerkinElmer). 293T cells

(#CRL-3216) were purchased from ATCC and were used in the passages 5–10. The culture medium consisted of high-glucose DMEM (#12800082, Gibco) supplemented with 10% serum (#10091-148, Gibco) and penicillin (100 U/mL)-streptomycin (100 µg/mL) (#15140-122, Gibco) and at 37 °C with 5% CO_2. Only 293T cells that were authenticated by STR profiling and tested negative for mycoplasma were used in this study.

2.11 Animal Experiments

The mouse experiments and protocols were approved by the Shanghai Institute of Materia Medica (Approved No. 2025-04-LJ-202), and this study was carried out in accordance with the ARRIVE guidelines. Wild-type (no genetic modifications) C57BL/6J male mice (strain #202), aged 6–8 weeks, were obtained from Shanghai Shengchang Biotechnology Co., LTD (China). Upon arrival, all animals were confirmed to be specific pathogen-free (SPF) and in good health, based on the health monitoring certificates supplied by the vendor; their genotype was verified by the vendor's certification. The mice were housed in an SPF barrier facility at the Shanghai Institute of Materia Medica, under a 12/12 hours light/dark cycle at 22 ± 2 °C and 50% humidity, with 5 animals per individually ventilated cage. After a 1-week acclimatization period, during which no signs of infection, illness, or abnormal behavior were observed, the mice were subjected to experimental procedures. None of the animals had been exposed to any prior interventions (e.g., surgery, drug administration, or behavioral testing), and no genetic modifications were applied. To induce obesity, mice were fed a high-fat diet containing 60% kcal fat (#D12492, Research Diets), while the control group received a normal chow diet (Shanghai Shilin Biotechnology Co., LTD, China). The experimental unit was an individual mouse. Based on preliminary data, the epididymal adipose tissue from a single healthy mouse weighs approximately 0.4 g; since 2 g of adipose tissue was required per group for preparation of conditioned medium, each group comprised 5 mice (5 on chow diet and 5 on high-fat diet). A body weight exceeding 40 g was predefined as the criterion for successful obesity induction in the high-fat diet group. After 20 weeks of HFD feeding, all mice in this group met this threshold; therefore, no animals were excluded from the study. At the onset of obesity induction, the 10 mice were evenly allocated to the two groups based on comparable baseline body weight, without randomization, as this approach ensured balanced starting conditions between groups. The experimental and control groups were housed in separate cages under identical environmental conditions. The study was not blinded; both the first author and the corresponding authors were aware of the group assignments and animal conditions throughout the experiment. Following successful obesity induction, body weights were recorded. Statistical comparisons between the two groups were performed using a two-tailed unpaired Student's *t*-test in GraphPad Prism (v8.0.1). Body weight data are presented as mean ± SEM for each group.

2.12 Euthanasia of Mice

At the end of the animal experiment, mice were euthanized by gradual CO_2 (Shanghai Central Gases) inhalation using an SMQ-I type asphyxiation chamber (Shanghai Tianhuan Science Develop Co., LTD, China). CO_2 was introduced into the chamber at a displacement rate of 50% of the chamber volume per minute for 1.5 minutes, then the gas flow was maintained for another 1.5 minutes. Death was confirmed by observation of cardiac arrest, cessation of respiration, and fixed dilated pupils for at least 10 minutes.

2.13 Cell Viability Assay

BMDMs were differentiated from bone marrow monocytes in 10-cm dishes with M-CSF-containing medium for 7 days. After differentiation, cells were detached and seeded into 96-well plates at a density of 2×10^4 cells per well. Following 12 h of attachment, cells were treated with various concentrations of LJ-6 (0–20 µM) for 12 h, and then stimulated with LPS (100 ng/mL) for an additional 12 h. Subsequently, 10 µL of Cell Counting Kit-8 (CCK-8) enhanced solution (#MA0218, Meilunbio) was added to each well, and the plates were incubated at 37 °C for 1 h. Absorbance at 450 nm was measured using SpectraMax M5 Microreader (Molecular Devices). Cell viability was calculated relative to LJ-6 untreated control cells (set as 100%).

2.14 Lactate Dehydrogenase (LDH) Cytotoxicity Assay

BMDMs were seeded and treated with LJ-6 and LPS as described in Section 2.13. 293T cells were seeded into 96-well plates at a density of 5×10^4 cells per well and culture to approximately 90% confluence. Medium without cell (background group) and maximum LDH release control cells (without LJ-6) were also included. One hour before the end of the experiment, the maximum release control wells were treated with 15 µL of LDH release reagent (supplied with the kit, #C0017, Beyotime) to achieve complete lysis of the cells. At the end of treatment, the plate was centrifuged at 400 ×g for 5 minutes. An aliquot of 120 µL of supernatant from each well was carefully transferred to a new 96-well plate. Subsequently, 60 µL of the LDH detection working solution was added to each well. The plate was incubated for 30 minutes at room temperature in the dark. Absorbance was measured at 490 nm using a SpectraMax M5 microplate reader, with 620 nm as the reference wavelength. Culture medium without cells served as a blank control to subtract background absorbance. For each sample, the background-subtracted absorbance was divided by that of the maximum release control (also background-subtracted) to calculate the percentage of LDH release.

2.15 Cycloheximide (CHX) Chase Assay

BMDMs were cultured in 12-well plates and stimulated with LPS (100 ng/mL) for 12 h to induce HIF-1α expression. Then, cells were treated with 10 μg/mL cycloheximide (CHX, #HY-12320, MedChemExpress) in the presence of either DMSO (vehicle control) or LJ-6 (10 μM). Cells were harvested at 0, 5, 10, 15, 20, and 25 minutes after CHX addition, and the protein sample was separated by SDS-PAGE and subjected to Western blotting analysis with anti-HIF-1α and anti-β-actin antibodies.

2.16 Statistical Analysis

Data are shown as mean ± SEM throughout. Statistical comparisons between two experimental groups were conducted using Student's unpaired, two-tailed *t*-test. For analyses involving three or more groups, one-way ANOVA was carried out with GraphPad Prism.

3. Results

3.1 Identification of LJ-6 as a Potent Anti-Inflammatory Lead Compound From a Natural Product Library

Chronic inflammation is a hallmark of obesity and a key driver of its associated metabolic complications. In adipose tissue, infiltrating macrophages orchestrate this inflammatory response, largely through the overproduction of cytokines such as IL-1β, which critically promotes insulin resistance and metabolic dysfunction. Targeting macrophage-mediated inflammation, and in particular the IL-1β pathway, thus represents a promising therapeutic avenue.

To identify novel anti-inflammatory agents, we performed an initial screen of a library of 42 natural compounds. Using LPS-stimulated RAW 264.7 macrophages, we evaluated each compound at 5 μM, focusing on the suppression of IL-1β expression. Several compounds showed modest activity (**Supplementary Table 1**), but one, LJ-6 (Fig. 1A, library ID D8) with IUPAC name (E)-3-(4-hydroxyphenyl)-1-(5-methoxy-2,2-dimethylchromen-8-yl)prop-2-en-1-one, stood out, inhibiting LPS-induced IL-1β expression by 71.9%. This marked effect, specifically on IL-1β, nominated LJ-6 as a promising lead for further mechanistic investigation of the HIF-1α/IL-1β axis.

3.2 Dose-Response and Cytotoxicity of LJ-6 in Primary Macrophages

To identify the hit compound, we performed a high-throughput screen using the RAW 264.7 murine macrophage cell line. This cell line serves as a standard and convenient *in vitro* tool owing to its robust and reproducible response to LPS stimulation. Nevertheless, considering that RAW 264.7 cells are a transformed cell line that may not fully replicate the phenotypic and functional features of primary macrophages, we proceeded to validate the activity of LJ-6 in a more physiologically relevant cell model. ATMs are major contributors to obesity-associated adipose tissue inflammation. Accumulating evidence indicates that monocyte-derived macrophages, rather than tissue-resident populations, represent the predominant pathogenic subset driving this inflammatory process [39,40,41,42]. Consistent with this pathological origin, bone marrow-derived macrophages (BMDMs), which are differentiated from bone marrow monocytes under the stimulation of M-CSF, were utilized as a more relevant cell model compared to the RAW 264.7 cell line.

To bridge the gap between the immortalized RAW 264.7 screen and the physiologically relevant primary cells, we first determined the potency and safety profile of LJ-6 (structure shown in Fig. 1A) in BMDMs. BMDMs were treated with a broad concentration range of LJ-6 (0.156–20 μM). Quantitative PCR analysis of *Il1b* mRNA revealed a steep dose-response curve, with statistically significant suppression commencing at 0.625 μM (Fig. 1B). Non-linear regression analysis of the inhibition data yielded an IC_{50} value of 7.84 μM for LJ-6-mediated IL-1β suppression (Fig. 1C). To exclude the possibility of non-specific effects arising from cell damage, we concurrently assessed cell viability and membrane integrity. The CCK-8 assay demonstrated that LJ-6 maintained BMDM viability at concentrations up to 10 μM, with a mild but significant reduction observed only at the highest tested concentration of 20 μM (Fig. 1D). Consistently, lactate dehydrogenase (LDH) release into the culture medium, a marker of cytotoxicity, remained unchanged across the 0.156–10 μM range and became significantly elevated only at 20 μM (Fig. 1E). These data indicate that LJ-6 exerts its anti-inflammatory activity within a concentration window (≤10 μM) devoid of non-specific cytotoxic effects. Based on these results, 5 μM and 10 μM were selected as the optimal non-cytotoxic concentrations for subsequent mechanistic investigations.

3.3 LJ-6 Suppresses IL-1β in LPS-induced Primary Macrophages

Having established the effective and safe dose range, we next validated the anti-inflammatory efficacy of LJ-6 in the LPS-stimulated BMDM model at the selected concentrations. BMDMs were pretreated with LJ-6 for 12 hours prior to stimulation with LPS for an additional 12 hours to model a pro-inflammatory challenge. As shown in Fig. 2, LJ-6 treatment induced a concentration-dependent reduction in LPS-induced mRNA expression for key pro-inflammatory mediators, which included significant decreases in *Il1b*, *Il6*, *Nos2*, and *Ccl2* gene expression (Fig. 2A–D), indicating a broad suppressive effect on the inflammatory gene program.

We next focused on IL-1β, a key cytokine in metabolic inflammation. Consistent with the transcriptional data, LJ-6 markedly reduced the intracellular levels of pro-IL-1β (Fig. 2E). Densitometric quantification confirmed this dose-dependent inhibition (Fig. 2F). Notably, detectable

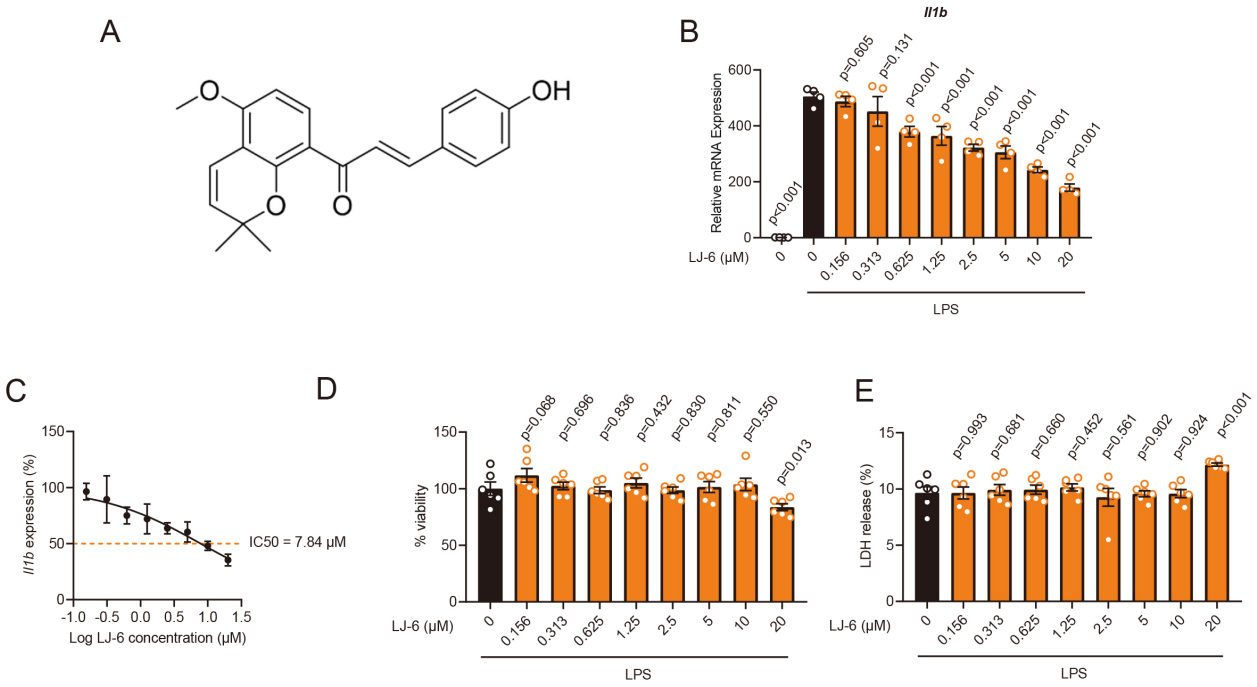

Fig. 1. Dose-response, potency, and cytotoxicity profile of LJ-6 in BMDMs. (A) Chemical structure of LJ-6. (B) BMDMs were pretreated with indicated concentrations of LJ-6 (0–20 μM) for 12 hours, followed by LPS (100 ng/mL) stimulation for 12 hours. *Il1b* mRNA expression was measured by qPCR; the LPS-only group (0 μM LJ-6) was taken as the control group for *p*-value calculation, n = 4 biological replicates. (C) Non-linear regression analysis of the inhibition data from (B), yielding an IC_{50} value of 7.84 μM. (D) Cell viability was assessed by CCK-8 assay. BMDMs were pretreated with indicated concentrations of LJ-6 (0–20 μM) for 12 hours, followed by LPS (100 ng/mL) stimulation for 12 hours, n = 6 biological replicates. (E) Cytotoxicity was evaluated by measuring LDH release in the culture supernatant. BMDMs were pretreated with indicated concentrations of LJ-6 (0–20 μM) for 12 hours, followed by LPS (100 ng/mL) stimulation for 12 hours, n = 6 biological replicates. Data are presented as mean ± SEM. BMDMs, bone marrow-derived macrophages; LPS, lipopolysaccharide; CCK-8, Cell Counting Kit-8.

secretion of mature IL-1β into the culture supernatant required a secondary stimulus (ATP) following LPS priming, a standard model of inflammasome activation. Under these conditions, LJ-6 pretreatment significantly reduced the extracellular levels of secreted IL-1β (Fig. 2G). Under the same ATP stimulation conditions, LJ-6 did not cause detectable cytotoxicity as assessed by LDH release (**Supplementary Fig. 2**). The parallel reduction in both intracellular protein levels (Fig. 2E,F) and secreted cytokine levels (Fig. 2G) suggests that LJ-6 primarily acts by suppressing IL-1β synthesis, rather than by specifically interfering with its processing or secretion pathways.

Collectively, these findings demonstrate that the natural compound LJ-6 effectively inhibits the LPS-induced expression and production of IL-1β, along with other critical inflammatory genes, in primary macrophages, underscoring its potential as an inhibitor of macrophage-driven inflammation.

3.4 LJ-6 Inhibits IL-1β in Macrophages Exposed to an Obese Adipose Tissue Microenvironment

To evaluate the anti-inflammatory effect of LJ-6 in a more physiologically relevant obesity context, we employed an *ex vivo* model based on adipose tissue-conditioned medium (AT CM). Chow-fed healthy mice and high-fat diet (HFD)-fed mice with obesity (20-week feeding regimen; Fig. 3A) were used to obtain AT CM, which retains soluble factors released by the adipose tissue *in vivo* (Fig. 3B). BMDMs were then treated with AT CM to mimic the local inflammatory milieu of lean or obese adipose tissue.

AT CM from obese mice significantly upregulated the levels of key pro-inflammatory genes (*Il1b*, *Nos2*, and *Ccl2*) in BMDMs, compared with CM from lean mice, confirming that obesity shifts the adipose secretome toward a pro-inflammatory state (Fig. 3C–F). Pre-treatment with LJ-6 markedly attenuated this obesity-associated inflammatory response, reducing the expression of *Il1b*, *Nos2*, and *Ccl2* (Fig. 3C–F). At the protein level, LJ-6 at 5 μM showed a trend toward reducing the intracellular accumulation of IL-1β induced by obese AT CM, while the 10 μM dose produced a statistically significant reduction, as demonstrated by Western blotting analysis and its quantification (Fig. 3G,H).

These data indicate that LJ-6 can effectively counteract the pro-inflammatory signals emanating from obese adi-

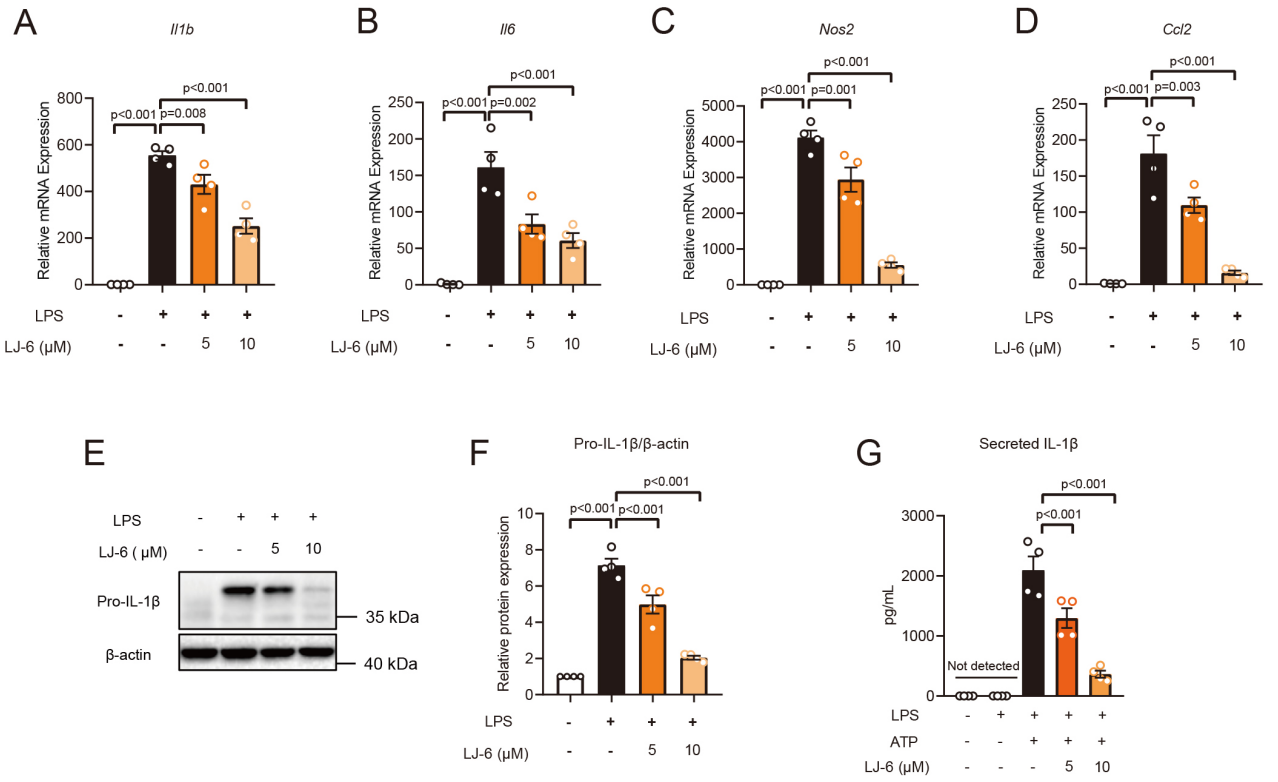

Fig. 2. LJ-6 inhibits LPS-induced IL-1β production in BMDMs. (A–D) mRNA expression levels of *Il1b* (A), *Il6* (B), *Nos2* (C), and *Ccl2* (D) in BMDMs, n = 4 biological replicates. (E) Representative Western blotting analysis of IL-1β protein expression. (F) Quantification of the Western blotting data shown in (E) is presented, n = 4 independent experiments. (G) Secreted IL-1β levels in culture medium, BMDMs received a 12-hour pretreatment with LJ-6, after which they were exposed to LPS (100 ng/mL) for 12 hours and then to ATP (2 mM) for an additional 30 minutes, n = 4 biological replicates. Values represent means ± SEM.

pose tissue in an *ex vivo* setting, highlighting its potential utility in obesity-associated adipose tissue inflammation.

3.5 LJ-6 Suppresses IL-1β Through Direct Binding to HIF-1α

Given the central role of HIF-1α in driving IL-1β expression during pro-inflammatory macrophage activation and in obese adipose tissue remodeling, we next investigated whether LJ-6 modulates this pathway. In LPS-stimulated BMDMs, LJ-6 treatment dose-dependently reduced HIF-1α protein levels (Fig. 4A,B), while also decreasing IL-1β expression (Fig. 4A,C), suggesting that HIF-1α may be involved in its anti-inflammatory action. To test this hypothesis, we co-treated cells with LJ-6 and pharmacological BAY 87-2243 (HIF-1α inhibitor). The inhibitor abrogated the suppressive effect of LJ-6 on IL-1β mRNA (Fig. 4D), indicating that LJ-6 inhibits IL-1β in a HIF-1α-dependent manner.

To further investigate whether LJ-6 modulates HIF-1α protein stability, we performed a cycloheximide (CHX) chase assay. LJ-6 treatment significantly accelerated the degradation of HIF-1α protein in BMDMs, indicating that LJ-6 promotes HIF-1α instability (Fig. 4E). Additionally, to obtain direct biophysical evidence for the interaction between LJ-6 and HIF-1α, we performed a cellular thermal shift assay (CETSA), and found LJ-6 treatment markedly enhanced the thermal stability of endogenous HIF-1α in BMDM cell lysates (Fig. 4F), providing direct evidence that LJ-6 interacts with HIF-1α in a biological context.

To delineate the molecular details of this interaction, we performed molecular docking followed by MD simulations. Global docking of LJ-6 against HIF-1α generated 97 poses, which were refined by 10-ns MD and MM/GBSA scoring. The top 5 poses underwent extended 500-ns MD simulations, from which the most stable complex was selected for a final 1000-ns simulation. The trajectory confirmed that LJ-6 stably occupies a binding pocket flanked by residues Tyr92 and His197 (Fig. 4G and **Supplementary Fig. 6**, Supporting Information). Specifically, the chalcone carbonyl of LJ-6 forms a hydrogen bond with His197, while its B-ring engages Tyr92 *via* cation-π interaction, suggesting a direct and specific binding mode.

To functionally validate this interaction, we introduced Y92A and H197A mutations into HIF-1α and measured its transcriptional activity using a hypoxia-response element (HRE)-driven luciferase reporter. Under the same experimental conditions, LJ-6 did not cause detectable cytotoxicity as assessed by LDH release (**Supplementary**

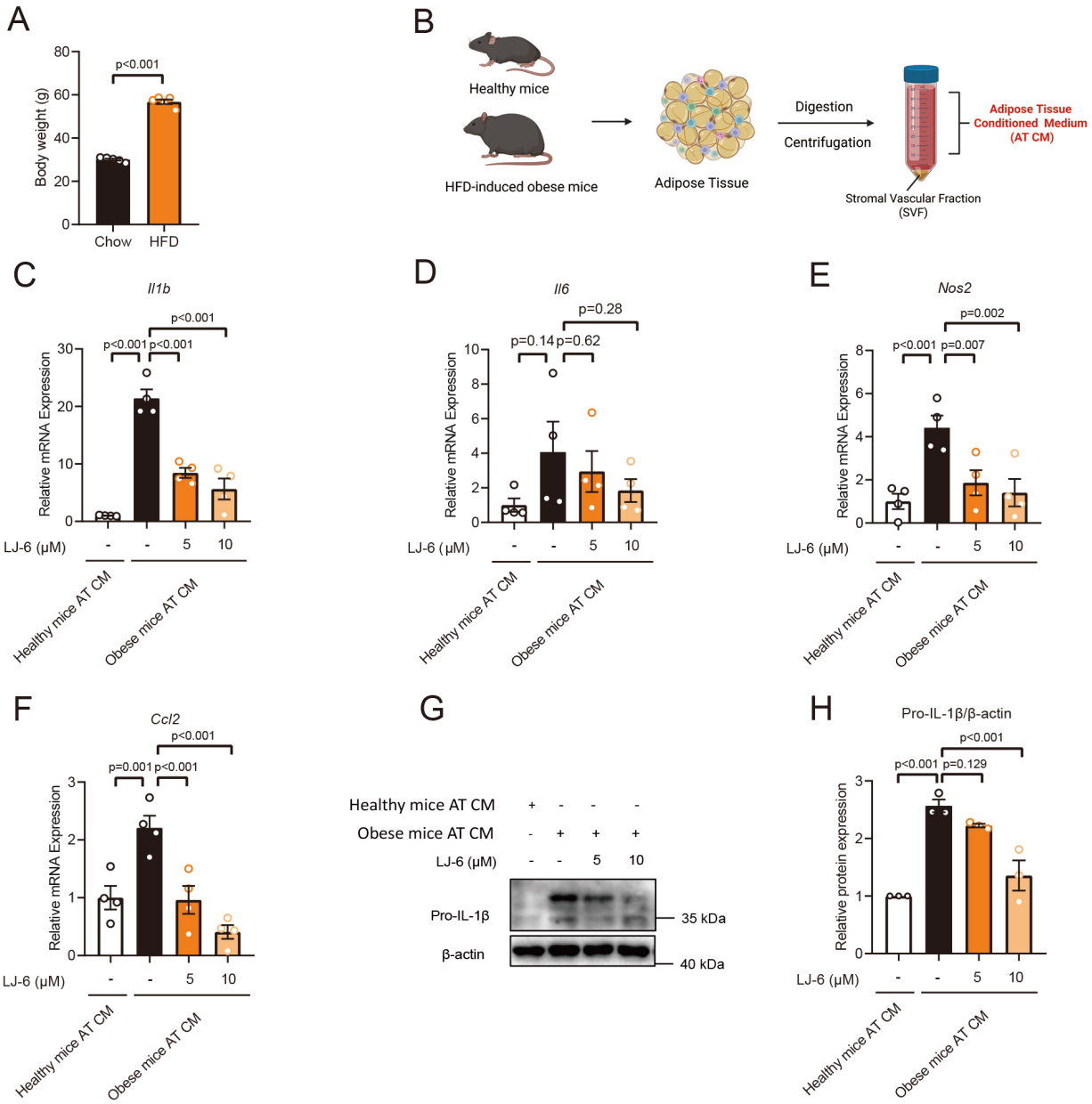

Fig. 3. LJ-6 inhibits conditioned medium-induced IL-1β production in BMDMs. (A) Body weights of lean (chow-fed) and obese (HFD-fed) mice after 20 weeks, n = 5 animals per group. The mean body weight of healthy mice were 30.0 g, the mean body weight of obese mice were 56.8 g, and the effect size, expressed as the mean difference between the two groups, was calculated with a 95% confidence interval of [24.08, 29.40]. (B) Schematic of adipose tissue-conditioned medium (AT CM) collection. (C–F) The expression levels of pro-inflammatory genes, namely *Il1b* (C), *Il6* (D), *Nos2* (E), and *Ccl2* (F) in BMDMs treated with AT CM from lean or obese mice, with or without LJ-6 pre-treatment, n = 4 biological replicates. (G) Representative immunoblots depicting intracellular IL-1β protein abundance. (H) Quantification of the Western blotting data shown in (G) is presented, n = 3 independent experiments. BMDMs received a 12-hour pretreatment with LJ-6 (or vehicle control), followed by 4-hour (for mRNA analysis) or 12-hour (for protein analysis) incubation with AT CM. Values are mean ± SEM. HFD, high-fat diet.

Fig. 3, Supporting Information). While LJ-6 effectively inhibited luciferase activity induced by wild-type HIF-1α, it failed to suppress signals from either mutant (Fig. 4H–J), confirming that both residues are essential for LJ-6-mediated inhibition.

Together, these data demonstrate that LJ-6 binds directly to HIF-1α at Tyr92 and His197, destabilizes HIF-1α protein, and thereby suppresses IL-1β expression in macrophages.

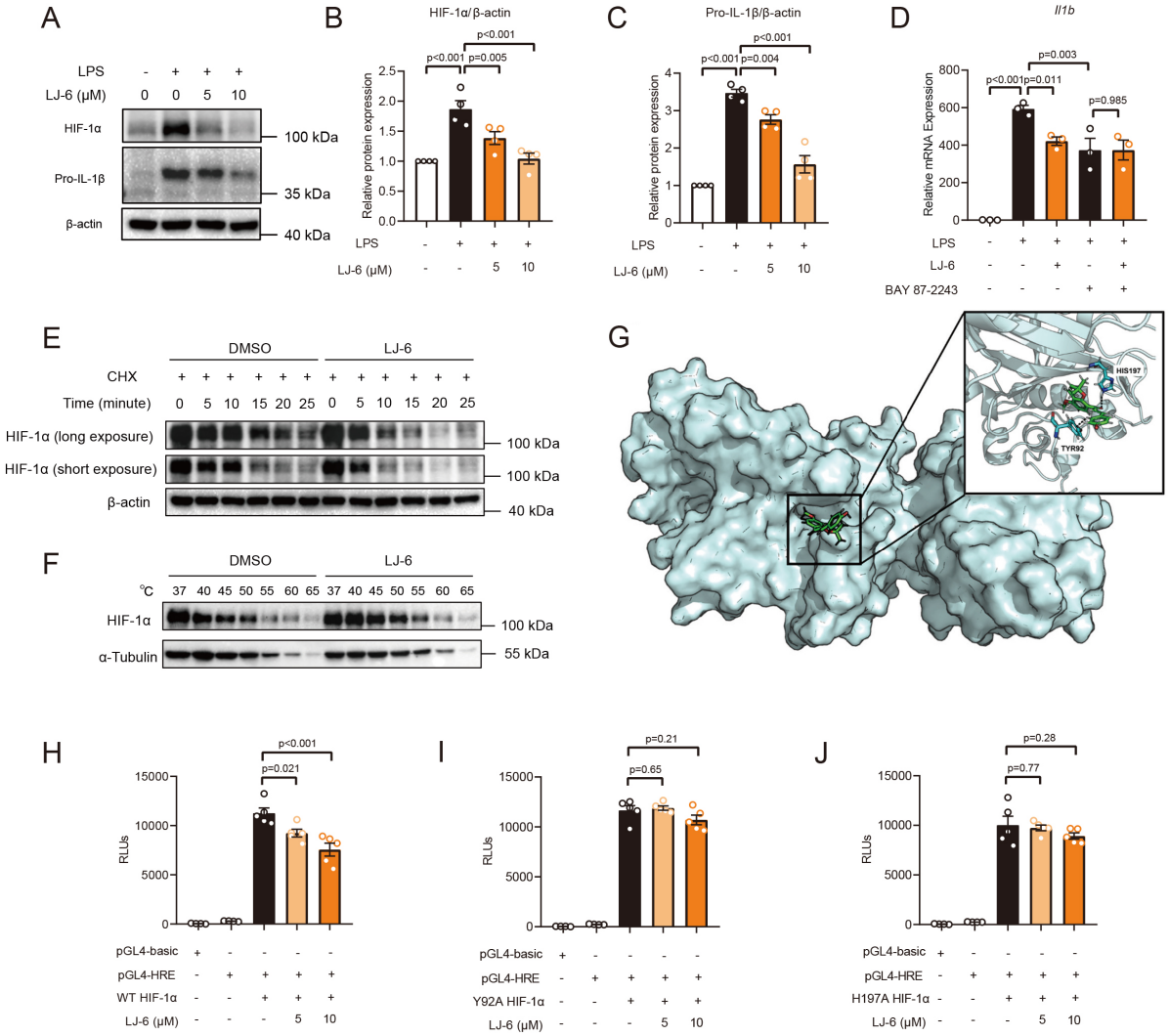

Fig. 4. LJ-6 reduces IL-1β through HIF-1α. (A) Representative immunoblots showing HIF-1α and IL-1β expression in BMDMs. (B,C) Quantification of HIF-1α (B) and IL-1β (C) protein levels from (A), n = 4 independent experiments. (D) *Il1b* mRNA expression in BMDMs pre-treated with LJ-6 (5 μM) and/or BAY 87-2243 (10 μM, #HY-15836, MedChemExpress) for 12 h, followed by LPS (100 ng/mL) for 12 h, n = 3 biological replicates. (E) Cycloheximide (CHX) chase assay. (F) Cellular thermal shift assay (CETSA). (G) Predicted binding mode of **LJ-6** (green sticks) in the HIF-1α pocket (surface representation). Key interactions with Tyr92 and His197 (sticks) are shown. (H–J) HRE-driven luciferase reporter activity was measured in 293T cells transfected with WT or mutant HIF-1α constructs (Y92A or H197A) along with the HRE-luciferase plasmid, following 12 hours of LJ-6 treatment or vehicle control, n = 5 biological replicates. Data are mean ± SEM.

4. Discussion

This study identifies the natural compound LJ-6 as a novel, direct inhibitor of HIF-1α, which effectively suppresses the key pro-inflammatory axis HIF-1α/IL-1β of macrophages, suggesting its potential to mitigate IL-1β-driven adipose tissue inflammation. We validated its efficacy not only in a canonical LPS-stimulation model but, more importantly, in a pathophysiologically relevant model using conditioned medium from obese adipose tissue, which reflects the complex secretome of the disease state. Mechanistically, we pinpoint Tyr92 (located in the PAS-A domain) and His197 (located in the inter-domain linker region preceding PAS-B) as the direct binding site for LJ-6 within the HIF-1α protein. This interaction is critical for its inhibition of HIF-1α protein stability and transcriptional activity, resulting in downregulation of *Il1b*. Our work thus provides both a novel chemical probe for dissecting HIF-1α signaling in immunometabolism and a compelling proof-of-concept in cellular and *ex vivo* models that pharmacologically disrupting this axis is a viable therapeutic strategy against obesity-related inflammation.

Chronic, low-grade inflammation driven by ATMs is a hallmark of metabolic dysfunction in obesity. While current weight-loss treatments (including GLP-1 receptor ag-

onists) are effective, they may not fully resolve the established inflammatory state of adipose tissue. This "inflammatory memory" can create a microenvironment conducive to metabolic dysfunction and even weight regain. Therefore, agents that directly modulate the macrophage inflammatory program, either independently or in synergy with weight-loss strategies, address a critical unmet need. LJ-6 represents a candidate of this class with potential for "causal" anti-inflammatory intervention that warrants further investigation *in vivo*.

We employed a dual-model strategy to validate LJ-6. Its potent activity in the classic LPS model confirmed its intrinsic anti-inflammatory capacity. However, the inflammatory milieu in obesity is a complex network of signals from adipocytes, immune cells, and stromal components. Our use of conditioned medium from obese adipose tissue, which incorporates this pathophysiological secretome, provides more compelling translational evidence. LJ-6's efficacy in this model suggests it can counteract inflammation driven by the synergistic action of multiple obesity-released factors, moving beyond single-pathway inhibition and suggesting its potential utility in a complex *in vivo* setting.

The central mechanistic finding of this study is the identification of HIF-1α as LJ-6's direct target. In obese adipose tissue, hypoxia stabilizes HIF-1α in ATMs, making it a master transcriptional regulator linking hypoxia to inflammation, including direct transactivation of IL-1β. Our data delineate a clear pathway: LJ-6 reduces HIF-1α protein levels, and its effect depends on HIF-1α. Crucially, molecular docking and mutagenesis experiments revealed that LJ-6 binds to residues Tyr92 (located in the PAS-A domain) and His197 (located in the inter-domain linker region preceding PAS-B) of HIF-1α. Given that the PAS-B domain is essential for heterodimerization with HIF-1β (ARNT) to form the transcriptionally active complex, we propose that LJ-6 likely inhibits HIF-1α function by disrupting this critical protein-protein interaction, a mechanism that differs from inhibitors that promote HIF-1α degradation. This finding provides a novel chemical scaffold and a rationale for developing specific inhibitors of the HIF-1α/HIF-1β dimerization interface.

LJ-6 is a chalcone derivative, a class of compounds known for anti-inflammatory properties typically mediated through NF-κB or MAPK pathways. Our discovery that LJ-6 acts via direct HIF-1α inhibition reveals a novel mechanism of action for chalcones, broadening their known pharmacological scope. This highlights their potential for treating conditions in which hypoxia-inflammation crosstalk is pivotal, such as obesity, atherosclerosis, and cancer. As a natural product, LJ-6 may offer favorable biocompatibility, supporting its further development as a lead compound.

A notable observation in our study is that LJ-6 also reduced the expression of other pro-inflammatory genes, including *Il6*, *Nos2*, and *Ccl2*, alongside *IL-1β* (Fig. 2A–D). While our mechanistic data firmly establish that HIF-1α is required for LJ-6-mediated suppression of *IL-1β* (Fig. 4D–J), the molecular basis for the inhibition of these additional inflammatory mediators remains unknown and falls beyond the scope of the current investigation. Several possibilities could be considered. For instance, since HIF-1α is a master transcriptional regulator, the downregulation of Il6 or Nos2 might be secondary to HIF-1α inhibition or a downstream effect of reduced IL-1β signaling. Alternatively, as a chalcone derivative, LJ-6 might directly engage other signaling pathways, such as NF-κB or MAPK, to exert broader effects. Unbiased transcriptomic or phospho-proteomic profiling would be required to distinguish these possibilities in future studies. Importantly, however, our central finding, that LJ-6 serves as a direct HIF-1α-binding chemical probe to functionally validate the therapeutic potential of targeting the HIF-1α/IL-1β axis, remains robust, irrespective of whether its effects on other genes are direct or indirect.

5. Limitations

This study has limitations that outline clear future directions. First, the *in vivo* efficacy and pharmacokinetic profile of LJ-6 in animal models of diet-induced obesity require evaluation. Second, while we focused on IL-1β, HIF-1α regulates a broad transcriptional program. Global transcriptomic or proteomic analyses are needed to fully define LJ-6's impact on the macrophage phenotype. Third, the precise biochemical consequence of LJ-6 binding, whether it primarily disrupts dimerization, affects co-activator recruitment, or influences protein stability, warrants further investigation via co-immunoprecipitation and degradation pathway assays.

6. Conclusions

Collectively, these findings establish LJ-6 as a previously unrecognized direct HIF-1α inhibitor that acts within macrophages. We demonstrate that LJ-6 effectively suppresses the HIF-1α/IL-1β axis, thereby reducing IL-1β expression in both canonical (LPS) and pathophysiologically relevant cellular and *ex vivo* models. Notably, LJ-6 also reduced the expression of other inflammatory genes (e.g., *Il6*, *Nos2* and *Ccl2*), although the mechanisms underlying these additional effects require further investigation. Mechanistically, LJ-6 exerts this effect through direct engagement of HIF-1α at Tyr92 and His197, which consequently suppresses its transcriptional output. Our work provides mechanistic insights that may inform future translational studies. At the mechanistic level, it furnishes direct pharmacological evidence that specifically targeting the HIF-1α/IL-1β axis in macrophages is a viable strategy to counteract adipose tissue inflammation, a core driver of obesity-related metabolic dysfunction, as shown in cellular and *ex vivo* models. Translationally, LJ-6 emerges as a promising therapeutic lead. It serves as a prototype compound for further optimization and *in vivo* testing toward the goal of resolving metabolic inflammation.

Taken together, by discovering and characterizing LJ-6, our work not only deepens the mechanistic understanding of HIF-1α's role in metabolic inflammation but also provides a chemical starting point for developing targeted immunometabolic strategies against obesity and its comorbidities.

Availability of Data and Materials

All data reported in this study can be obtained from the corresponding authors upon reasonable request.

Author Contributions

HJ, JinL, and CP designed the research study. The experiments were performed by MG, ML, AC, SD, JG, SshaL, DJ, YS, and XyueW. Data were analyzed by JiaL, SfeiL and RW. Chemistry-related work, including compound library construction and synthesis, was conducted by AC, DJ, YS, and XyiW. Molecular docking and dynamics simulations were carried out by SD and JG. The manuscript was written by CP and JinL. All authors reviewed the manuscript and approved the final version. All authors contributed to editorial changes in the manuscript. All authors have participated sufficiently in the work and agreed to be accountable for all aspects of the work.

Ethics Approval and Consent to Participate

This study was carried out in strict accordance with the Chinese national standard GB/T 35892-2018 and the ARRIVE guidelines. The protocol was specifically approved by the Animal Ethics Committee of the Shanghai Institute of Materia Medica (Approval No. 2025-04-LJ-202).

Acknowledgment

We gratefully acknowledge the assistance and instruction in the animal experiment provided by Dr. Liya Jing and Dr. Huan Ma of the Shanghai Institute of Materia Medica. The Graphical abstract was created in BioRender. Jiang, H. (2026) https://BioRender.com/pcmz925.

Funding

This research was funded by Natural Science Foundation of Hunan Province, grant number 2024JJ5308; Research Foundation of Education Bureau of Hunan Province, China, grant number 23B0366; Central Guiding Local Science and Technology Development Fund Projects, grant number 2025ZY01043; Research Funds of Hangzhou Institute for Advanced Study, UCAS, grant number B05006C021007.

Conflicts of Interest

The authors declare no conflicts of interest.

Declaration of AI and AI-Assisted Technologies in the Writing Process

During the preparation of this work the authors used deepseek-V3 in order to check spelling and grammar. After using this tool, the authors reviewed and edited the content as needed and take full responsibility for the content of the publication.

Supplementary Material

Supplementary material associated with this article can be found, in the online version, at https://doi.org/10.31083/FBL53391.

References

[1] Kong Y, Yang H, Nie R, Zhang X, Zuo F, Zhang H, et al. Obesity: pathophysiology and therapeutic interventions. Molecular Biomedicine. 2025; 6: 25. https://doi.org/10.1186/s43556-025-00264-9

[2] Klein S, Gastaldelli A, Yki-Järvinen H, Scherer PE. Why does obesity cause diabetes? Cell metabolism. 2022; 34: 11–20. https://doi.org/10.1016/j.cmet.2021.12.012

[3] Abdelsattar M, Elseady Y, Hendawy A, Diab AE, Awadin WF, Eldesoqui M. Impact of Peganum Harmala/Zinc Oxide Nanoparticles on Thyroid and Pancreatic Function in Obese Rats: A Biochemical and Physiological Analysis. International Journal of Pharmacology. 2024; 20: 981–990. https://doi.org/10.3923/ijp.2024.981.990

[4] Wang JH, Lu HC, Wu ZH, Chang TC. Integrative Analysis of BMI and Gene Expression Reveals Molecular Interactions Underlying Cancer Progression. Frontiers in Bioscience (Landmark Edition). 2025; 30: 43294. https://doi.org/10.31083/FBL43294

[5] Varra FN, Varras M, Varra VK, Theodosis-Nobelos P. Molecular and pathophysiological relationship between obesity and chronic inflammation in the manifestation of metabolic dysfunctions and their inflammation-mediating treatment options (Review). Molecular Medicine Reports. 2024; 29: 95. https://doi.org/10.3892/mmr.2024.13219

[6] Higos R, Renzi G, Taillandier P, Merabtene F, Rouault C, Abatan JB, et al. How Adipocytes Orchestrate Inflammation Within Adipose Tissue? Biomolecules. 2025; 16: 59. https://doi.org/10.3390/biom16010059

[7] Peng C, Chen J, Wu R, Jiang H, Li J. Unraveling the complex roles of macrophages in obese adipose tissue: an overview. Frontiers of Medicine. 2024; 18: 205–236. https://doi.org/10.1007/s11684-023-1033-7

[8] Li X, Ren Y, Chang K, Wu W, Griffiths HR, Lu S, et al. Adipose tissue macrophages as potential targets for obesity and metabolic diseases. Frontiers in Immunology. 2023; 14: 1153915. https://doi.org/10.3389/fimmu.2023.1153915

[9] Ahmed B, Sultana R, Greene MW. Adipose tissue and insulin resistance in obese. Biomedicine & Pharmacotherapy = Biomedecine & Pharmacotherapie. 2021; 137: 111315. https://doi.org/10.1016/j.biopha.2021.111315

[10] Moiz A, Filion KB, Tsoukas MA, Yu OH, Peters TM, Eisenberg MJ. Mechanisms of GLP-1 Receptor Agonist-Induced Weight Loss: A Review of Central and Peripheral Pathways in Appetite and Energy Regulation. The American Journal of Medicine. 2025; 138: 934–940. https://doi.org/10.1016/j.amjmed.2025.01.021

[11] Miranda AMA, McAllan L, Mazzei G, Andrew I, Davies I, Ertugrul M, et al. Selective remodelling of the adipose niche in obesity and weight loss. Nature. 2025; 644: 769–779. https://doi.org/10.1038/s41586-025-09233-2

[12] Hinte LC, Castellano-Castillo D, Ghosh A, Melrose K, Gasser

E, Noé F, et al. Adipose tissue retains an epigenetic memory of obesity after weight loss. Nature. 2024; 636: 457–465. https://doi.org/10.1038/s41586-024-08165-7

[13] Meier DT, de Paula Souza J, Donath MY. Targeting the NLRP3 inflammasome-IL-1β pathway in type 2 diabetes and obesity. Diabetologia. 2025; 68: 3–16. https://doi.org/10.1007/s00125-024-06306-1

[14] Tack CJ, Stienstra R, Joosten LAB, Netea MG. Inflammation links excess fat to insulin resistance: the role of the interleukin-1 family. Immunological Reviews. 2012; 249: 239–252. https://doi.org/10.1111/j.1600-065X.2012.01145.x

[15] Aladhami AK, Unger CA, Ennis SL, Altomare D, Ji H, Hope MC, 3rd, et al. Macrophage tumor necrosis factor-alpha deletion does not protect against obesity-associated metabolic dysfunction. FASEB Journal : Official Publication of the Federation of American Societies for Experimental Biology. 2021; 35: e21665. https://doi.org/10.1096/fj.202100543RR

[16] Peng C, Jiang H, Jing L, Yang W, Guan X, Wang H, et al. Macrophage SUCLA2 coupled glutaminolysis manipulates obesity through AMPK. Nature Communications. 2025; 16: 1738. https://doi.org/10.1038/s41467-025-57044-w

[17] Peiró C, Lorenzo Ó, Carraro R, Sánchez-Ferrer CF. IL-1β Inhibition in Cardiovascular Complications Associated to Diabetes Mellitus. Frontiers in Pharmacology. 2017; 8: 363. https://doi.org/10.3389/fphar.2017.00363

[18] Lin WW, Lu YC, Huang BC, Chuang CH, Cheng YA, Chen IJ, et al. Selective activation of pro-anti-IL-1β antibody enhances specificity for autoinflammatory disorder therapy. Scientific Reports. 2021; 11: 14846. https://doi.org/10.1038/s41598-021-94298-y

[19] Sharma M, Boytard L, Hadi T, Koelwyn G, Simon R, Ouimet M, et al. Enhanced glycolysis and HIF-1α activation in adipose tissue macrophages sustains local and systemic interleukin-1β production in obesity. Scientific Reports. 2020; 10: 5555. https://doi.org/10.1038/s41598-020-62272-9

[20] Sun K, Halberg N, Khan M, Magalang UJ, Scherer PE. Selective inhibition of hypoxia-inducible factor 1α ameliorates adipose tissue dysfunction. Molecular and Cellular Biology. 2013; 33: 904–917. https://doi.org/10.1128/MCB.00951-12

[21] Newman DJ, Cragg GM. Natural Products as Sources of New Drugs over the Nearly Four Decades from 01/1981 to 09/2019. Journal of Natural Products. 2020; 83: 770–803. https://doi.org/10.1021/acs.jnatprod.9b01285

[22] SWISS-MODEL Repository. Q16665 (HIF1A_HUMAN) Homo sapiens (Human): hypoxia-inducible factor 1-alpha. n.d. Available at: https://swissmodel.expasy.org/repository/uniprot/Q16665?range=11-357&template=4zpk.1.B (Accessed: 20 June 2026).

[23] Jorgensen WL, Chandrasekhar J, Madura JD, Impey RW, Klein ML. Comparison of simple potential functions for simulating liquid water. The Journal of Chemical Physics. 1983; 79: 926–935. https://doi.org/10.1063/1.445869

[24] Lindorff-Larsen K, Piana S, Palmo K, Maragakis P, Klepeis JL, Dror RO, et al. Improved side-chain torsion potentials for the Amber ff99SB protein force field. Proteins. 2010; 78: 1950–1958. https://doi.org/10.1002/prot.22711

[25] Best RB, Hummer G. Optimized molecular dynamics force fields applied to the helix-coil transition of polypeptides. The Journal of Physical Chemistry. B. 2009; 113: 9004–9015. https://doi.org/10.1021/jp901540t

[26] Hornak V, Abel R, Okur A, Strockbine B, Roitberg A, Simmerling C. Comparison of multiple Amber force fields and development of improved protein backbone parameters. Proteins. 2006; 65: 712–725. https://doi.org/10.1002/prot.21123

[27] Wang J, Cieplak P, Kollman PA. How well does a restrained electrostatic potential (RESP) model perform in calculating conformational energies of organic and biological molecules?. Journal of Computational Chemistry. 2000; 21: 1049–1074. https://doi.org/10.1002/1096-987X(200009)21:12<1049::AID-JCC3>3.0.CO;2-F

[28] Wang J, Wolf RM, Caldwell JW, Kollman PA, Case DA. Development and testing of a general amber force field. Journal of Computational Chemistry. 2004; 25: 1157–1174. https://doi.org/10.1002/jcc.20035

[29] Bowers KJ, Chow DE, Xu H, Dror RO, Eastwood MP, Gregersen BA, et al. Scalable algorithms for molecular dynamics simulations on commodity clusters. In Proceedings of the 2006 ACM/IEEE conference on Supercomputing. Association for Computing Machinery: Tampa, Florida. 2006. https://doi.org/10.1145/1188455.1188544

[30] Hoover W. Canonical dynamics: Equilibrium phase-space distributions. Physical Review. A, General Physics. 1985; 31: 1695–1697. https://doi.org/10.1103/physreva.31.1695

[31] Martyna GJ, Tobias DJ, Klein ML. Constant pressure molecular dynamics algorithms. The Journal of Chemical Physics. 1994; 101: 10–63. https://doi.org/10.1063/1.467468

[32] Predescu C, Lippert RA, Eastwood MP, Ierardi D, Xu H, Jensen MØ, et al. Computationally efficient molecular dynamics integrators with improved sampling accuracy. Molecular Physics. 2012; 110: 967–983. https://doi.org/10.1080/00268976.2012.681311

[33] Eberhardt J, Santos-Martins D, Tillack AF, Forli S. AutoDock Vina 1.2.0: New Docking Methods, Expanded Force Field, and Python Bindings. Journal of Chemical Information and Modeling. 2021; 61: 3891–3898. https://doi.org/10.1021/acs.jcim.1c00203

[34] Trott O, Olson AJ. AutoDock Vina: improving the speed and accuracy of docking with a new scoring function, efficient optimization, and multithreading. Journal of Computational Chemistry. 2010; 31: 455–461. https://doi.org/10.1002/jcc.21334

[35] O'Boyle NM, Banck M, James CA, Morley C, Vandermeersch T, Hutchison GR. Open Babel: An open chemical toolbox. Journal of Cheminformatics. 2011; 3: 33. https://doi.org/10.1186/1758-2946-3-33

[36] Santos-Martins D, He Y, Eberhardt J, Sharma P, Bruciaferri N, Holcomb M, et al. Meeko: Molecule Parametrization and Software Interoperability for Docking and Beyond. Journal of Chemical Information and Modeling. 2025; 65: 13045–13050. https://doi.org/10.1021/acs.jcim.5c02271

[37] Valdés-Tresanco MS, Valdés-Tresanco ME, Valiente PA, Moreno E. gmx_MMPBSA: A New Tool to Perform End-State Free Energy Calculations with GROMACS. Journal of Chemical Theory and Computation. 2021; 17: 6281–6291. https://doi.org/10.1021/acs.jctc.1c00645

[38] Wang E, Sun H, Wang J, Wang Z, Liu H, Zhang JZH, et al. End-Point Binding Free Energy Calculation with MM/PBSA and MM/GBSA: Strategies and Applications in Drug Design. Chemical Reviews. 2019; 119: 9478–9508. https://doi.org/10.1021/acs.chemrev.9b00055

[39] Cox N, Crozet L, Holtman IR, Loyher PL, Lazarov T, White JB, et al. Diet-regulated production of PDGFcc by macrophages controls energy storage. Science (New York, N.Y.). 2021; 373: eabe9383. https://doi.org/10.1126/science.abe9383

[40] Kim J, Chung K, Choi C, Beloor J, Ullah I, Kim N, et al. Silencing CCR2 in Macrophages Alleviates Adipose Tissue Inflammation and the Associated Metabolic Syndrome in Dietary Obese Mice. Molecular Therapy. Nucleic Acids. 2016; 5: e280. https://doi.org/10.1038/mtna.2015.51

[41] O'Brien CJO, Domingos AI. An anti-obesity immunotherapy? Science (New York, N.Y.). 2021; 373: 24–25. https://doi.org/10.1126/science.abj5072

[42] Hill DA, Lim HW, Kim YH, Ho WY, Foong YH, Nelson VL, et al. Distinct macrophage populations direct inflammatory versus physiological changes in adipose tissue. Proceedings of the National Academy of Sciences of the United States of America. 2018; 115: E5096–E5105. https://doi.org/10.1073/pnas.1802611115